# Why Are Viscosities Lower for Ionic Liquids with $-CH_2Si(CH_3)_3$ vs $-CH_2C(CH_3)_3$ Substitutions on the Imidazolium Cations?

**Hideaki Shirota* and Edward W. Castner, Jr.***

*Department of Chemistry and Chemical Biology, Rutgers, The State University of New Jersey, 610 Taylor Road, Piscataway, New Jersey 08854-8087*

*Received: July 17, 2005; In Final Form: September 1, 2005*

We have prepared novel room temperature ionic liquids (RTILs) with trimethylsilylmethyl (TMSiM)-substituted imidazolium cations and compared the properties of these liquids with those for which the TMSiM group is replaced by the analogous neopentyl group. The ionic liquids are prepared with both tetrafluoroborate ($BF_4^-$) and bis(trifluoromethylsulfonyl)imide ($NTf_2^-$) anions paired with the imidazolium cations. At 22 °C, the TMSiM-substituted imidazolium ILs have shear viscosities that are reduced by a factor of 1.6 and 7.4 relative to the alkylimidazolium ILs for the $NTf_2^-$ and $BF_4^-$ anions, respectively. To understand the effect of silicon substitution on the viscosity, the charge densities have been calculated by using density functional theory electronic structure calculations. The ultrafast intermolecular, vibrational, and orientational dynamics of these RTILs have been measured by using femtosecond optical heterodyne-detected Raman-induced Kerr effect spectroscopy (OHD-RIKES). The intermolecular dynamical spectrum provides an estimate of the strength of interactions between the ions in the RTILs, and provides a qualitative explanation for the observed reduction in viscosity for the silicon-substituted RTILs.

## 1. Introduction

Room temperature ionic liquids (RTILs) provide many exciting opportunities in chemistry, including possible use as replacements for volatile organic solvents in electrochemistry, enzyme catalysis, chemical synthesis, and radioactive waste handling.[1−9] The viscosities of RTILs are relatively high compared with those of common organic solvents. Organic solvents typically have room temperature viscosities ranging from 0.2 to 10 cP.[10] RTILs display a broad range of room temperature viscosities, from 10 to greater than $10^5$ cP.[11] The relatively high viscosities of RTILs can make common laboratory tasks such as filtration, decantation, and dissolution more difficult. More significantly, higher viscosities can lead to slower rates for diffusion-controlled reactions. One goal in designing new RTILs for laboratory use is to obtain lower room temperature viscosities.

It is possible to achieve control of viscosity, glass transition temperature, and other relevant liquid-state properties by making chemical modifications to either the anion or the cation of the IL. Changing the anion through a series of homologous cation RTILs can provide dramatic changes of the viscosity. In particular, use of either the bis(trifluoromethylsulfonyl)imide ($NTf_2^-$) or dicyanoamide ($DCA^-$) anions most often leads to the greatest drop in viscosity.[11,12] More precise control over a range of selected properties can be obtained by designing cations with modest changes to their side groups. The research teams of Cooper and Angell,[13] Miyazaki,[14] and Wishart[15] have demonstrated that both the melting points and viscosities of RTILs can be reduced by replacement of an alkyl group by a more flexible ether group. Dyson and co-workers demonstrated the effect of a cyano group substitution on the RTIL cation.[16]

**CHART 1. Chemical Structures of $MTMSiMIm^+$ and $MNPIm^+$**

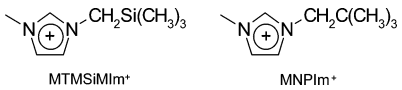


Silicon has lower electronegativity than carbon and silicon−carbon single bond lengths are substantially longer than the analogous carbon−carbon single bonds.[17,18] Silicon-containing polymers such as polysiloxanes display some of the lowest glass transition temperatures and melting points and are among the most flexible polymers known.[19] Because of the propensities for silicon-containing polymers to exhibit higher dimensional cross-linking, some are useful reagents for the preparation of highly functionalized silicate materials.[20,21] It is well-known that silicon is the second most abundant element on the earth, which is a fact worth considering because a major goal for many developers of ILs is to facilitate "green" or sustainable chemistry.

We have synthesized the novel silicon-containing imidazolium cation 1-methyl-3-trimethylsilylmethylimidazolium ($MTMSiMIm^+$) with a halide counterion, and created other RTILs by anion substitution with $BF_4^-$ and $NTf_2^-$ anions. For control experiments we have made the analogous alkylimidazolium cation, 1-methyl-3-neopentylimidazolium ($MNPIm^+$), with the same anions (Chart 1).

To obtain a preliminary understanding of what factors are significant in determining the intermolecular interactions and dynamics in the new RTILs, we have carried out three types of studies. Shear viscosities measured as a function of temperature provide a thermodynamic average of the interactions and show that Arrhenius behavior is not observed. Optical heterodyne-detected Raman-induced Kerr effect spectroscopy (OHD-RIKES) permits observation of the depolarized Raman projection of the intra- and intermolecular vibrational spectrum,

* Address correspondence to the authors at e-mail shirota@rutchem.rutgers.edu and castner@rutchem.rutgers.edu.

10.1021/jp053930j CCC: $30.25 
Published on Web 10/20/2005

**TABLE 1: Formula Weight (fw), van der Waals Molecular Volumes (*V*, estimated from the volume increments method), and Density (*d*) and Viscosity ($\eta$) at 22 °C for Each of the Four Imidazolium Ionic Liquids**

| ionic liquid | fw (g mol$^{-1}$)[a] | $V$ (Å$^3$)[a] | $d$ (g mL$^{-1}$)[b,c] | $\eta$ (cP)[b,d] |
|---|---|---|---|---|
| MTMSiMIm$^+$/BF$_4^-$ | 256 (C:169, A:87) | 206.9 (C: 180.2, A: 29.7) | 1.22 | 631 |
| MNPIm$^+$/BF$_4^-$ | 240 (C:153, A:87) | 196.5 (C: 166.8, A: 29.7) | 1.23 | 4638 |
| MTMSiMIm$^+$/NTf$_2^-$ | 449 (C:169, A:280) | 326.1 (C: 180.2, A: 145.9) | 1.46 | 98.3 |
| MNPIm$^+$/NTf$_2^-$ | 433 (C:153, A:280) | 312.7 (C: 166.8, A: 145.9) | 1.50 | 161 |

[a] C: cation. A: anion. [b] Values at 22 °C. [c] ±3%. [d] ±5%.

together with the longer time scale relaxational behavior arising from collective diffusive reorientation. The third element of this work includes gas phase density functional theory (DFT) calculations of the electronic ground state properties of the individual cation and anion components of these RTILs. Because the ultrafast intermolecular vibrational dynamics are strongly correlated with the intermolecular interactions, the comparison between the shear viscosity, electronic structure, and ultrafast intermolecular dynamics provides the first detailed insights into the microscopic factors that determine the liquid-state properties of these novel silicon-substituted imidazolium cation based RTILs.

## 2. Experimental Methods

**2.1. Preparation Methods and Viscosity Measurements.** Synthesis of the novel silicon containing RTILs MTMSiMIm$^+$/NTf$_2^-$ and MTMSiMIm$^+$/BF$_4^-$, and the RTILs with the analogous alkyl side group cation MNPIm$^+$/NTf$_2^-$ and MNPIm$^+$/BF$_4^-$, is accomplished with standard methods.[22−25] The reaction scheme is shown in eqs 1−3.

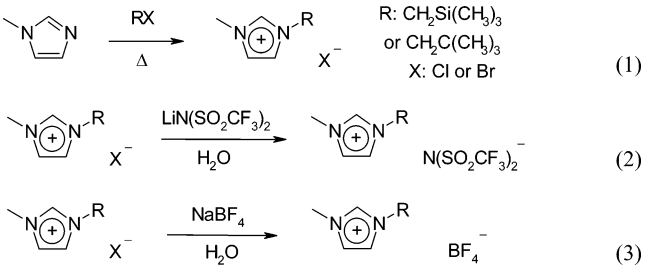


Reaction 1, where R is the trimethylsilylmethyl (TMSiM) group, gave a high yield for both the chloride (94%) and bromide (>99%) reactions under reflux at about 90 °C. In contrast, the reactivities of neopentyl (NP) chloride and NP bromide in reaction 1 were substantially reduced relative to those for the TMSiM chloride and TMSiM bromide. Even when the reaction was carried out at elevated temperatures under reflux at about 145 °C, no reaction was observed for NP chloride after 6 h. To increase the reaction yield, excess NP bromide (1.2 times excess relative to 1-methylimidazole) was used for reaction 1. Furthermore, the temperature and reaction time were increased to ∼145 °C and ∼45 h, respectively, providing a reaction yield of 34%. The anion exchange (methathesis) reactions 2 and 3 each gave yields of ∼80% for both MTMSiMIm$^+$/Cl$^-$ and MNPIm$^+$/Br$^-$. The newly synthesized RTILs were stirred over activated carbon for 12 h in acetonitrile solution. The RTILs were dried in vacuo at about 80 °C for 12 h. $^1$H NMR and electrospray ionization mass spectrometry (ESI-MS) were used to characterize the RTILs. Dilute methanol solutions of RTILs were used for ESI-MS and both positive and negative ion spectra were recorded. In addition to observations of the parent ions, clusters of 2-cation:anion and 2-anions:cation were observed. Further details of the respective syntheses and characterization are summarized in the Supporting Information.

Viscosity measurements were made on a Cambridge Applied Systems reciprocating electromagnetic piston viscometer, model ViscoLab 4100, with a detectable shear viscosity range of 0.2 to 10000 cP. Temperature control for the viscometer cell was achieved to ±0.1 K, using a Lauda RM-6 recirculating water bath. A 2-mL volumetric flask was tared and weighed on an analytical balance for the density measurements reported in Table 1.

**2.2. Femtosecond OHD-RIKES Measurements.** Femtosecond optical heterodyne-detected Raman-induced Kerr effect spectroscopy (OHD-RIKES) is a nonlinear optical polarization technique that measures the depolarized Raman signal from a transparent condensed phase sample in the time domain.[26,27] The sample polarization dynamics induced by a nonresonant pumping pulse are detected as an oscillatory decaying birefringence through crossed polarizers. Using OHD-RIKES, we can measure the dynamics in condensed phases on time scales ranging from 20 fs to 1 ns. The raw Kerr transients measured in the time domain data are converted to the low-frequency depolarized Raman spectrum by direct Fourier transform deconvolution over the range from 0.1 to 800 cm$^{-1}$.[27−29] A notable strength of this method is that intermolecular vibrational dynamics (∼0−300 cm$^{-1}$) can be recorded by femtosecond OHD-RIKES. Thus femtosecond OHD-RIKES has been used not only for simple molecular liquids,[26,27,30−32] but also for more complex condensed phases such as nanoporous glasses,[33,34] microemulsions,[35−37] and polymer liquids[38] and solutions,[36,39] as well as RTILs.[40−44]

The OHD-RIKES apparatus is based on previously published designs,[26,29] and the details of the instrument have been described elsewhere.[39,45] The instrument temporal response measured with a 200 $\mu$m KDP crystal was 37 ± 3 fs full width at half-maximum for these experiments, which is equivalent to a 24 ± 2 fs pulse, assuming a sech$^2$ line shape. The measured spectral bandwidth of the laser pulses was approximately 55 nm and centered at 805 nm. All the measurements were made at 296 ± 2 K. Scans with high time resolution of 4096 points at 0.5 $\mu$m/step were recorded for a time window of 13.66 ps. The slower orientational dynamics were captured in 100 ps scans with 5.0 $\mu$m per data point and in 730 ps scans with 50 $\mu$m per data point. Pure heterodyne signals were obtained by recording scans for ca. +1°and −1° rotations of the input polarizer, which are then added to remove the residual homodyne signal. Ten scans were averaged for the short time window transients (5 scans each for +1° and −1° rotations of the probe input polarizer), and 20 scans were averaged for the intermediate and long time windows (10 scans each for both the +1° and −1° rotations of the probe input polarizer).

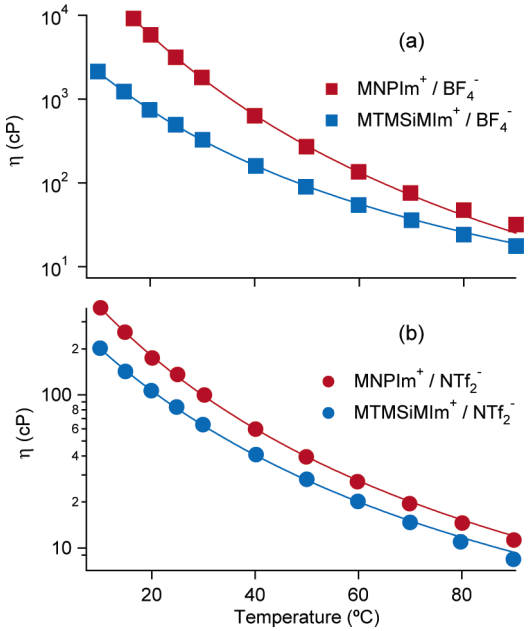


**Figure 1.** Temperature-dependent viscosities of (a) $MTMSiMIm^+/BF_4^-$ and $MNPIm^+/BF_4^-$ and (b) $MTMSiMIm^+/NTf_2^-$ and $MNPIm^+/NTf_2^-$. V-F-T fit curves are also shown.

**2.3. Density Functional Theory Calculations.** Calculations for geometry optimization and harmonic normal mode vibrational analysis for $MTMSiMIm^+$, $MNPIm^+$, $NTf_2^-$, and $BF_4^-$ were carried out with the Gaussian03 program package (Revision B.03).[46] Density functional theory (DFT) calculations were based on the Becke's three-parameter gradient-corrected exchange[47] and Lee−Yang−Parr gradient-corrected correlation functionals[48] (B3LYP), using the 6-311+G(d,p) basis set. The effective atom-centered charges were obtained by fitting the ground-state electrostatic potential, using the CHelpG algorithm.[49]

## 3. Results

**3.1. Viscosity and Density.** Figure 1 shows the temperature dependence of the shear viscosities for (a) $MTMSiMIm^+/BF_4^-$ and $MNPIm^+/BF_4^-$ and (b) $MTMSiMIm^+/NTf_2^-$ and $MNPIm^+/NTf_2^-$. The graphs of log viscosity vs temperature immediately show that these ILs do not display Arrhenius temperature behavior. Instead, behavior reminiscent of glassy or supercooled liquids is observed. The viscosities can be fit to the Vogel−Tamman−Fulcher (V-T-F) equation,[50]

$$\eta(T) = \eta_0 \exp\left(\frac{DT_0}{T - T_0}\right) \tag{4}$$

where $\eta$ is the shear viscosity, $T$ is the temperature, $\eta_0$ is a reference viscosity at which the exponential term is 0, $D$ is the fragility parameter, and $T_0$ is a characteristic temperature for which $\eta$ diverges. Table 1 summarizes the viscosity $\eta$ and density $d$ data at room temperature (22 °C). The room temperature densities of the $MTMSiMIm^+$ and the $MNPIm^+$ RTILs are similar. On the other hand, the viscosities are very different for the RTILs based on the $MTMSiMIm^+$ vs $MNPIm^+$ cations. $MTMSiMIm^+$ RTILs show shear viscosities that are about 1.6 and 7.4 times lower than $MNPIm^+$ RTILs with the $NTf_2^-$ and $BF_4^-$ anions, respectively. Table 1 also lists the molecular volumes $V$ for the component cations and anions,

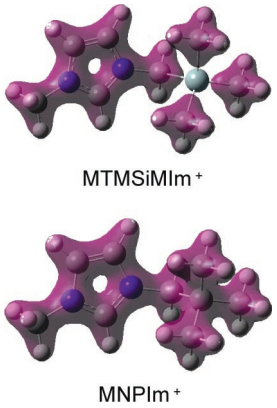


**Figure 2.** Optimized structures and total electron densities of $MTMSiMIm^+$ and $MNPIm^+$ cations calculated at the B3LYP/6-311+G(d,p) level. Isodensity surfaces are plotted at a value of 0.1.

which are estimated from the method of van der Waals increments.[51,52] Because values for some van der Waals increments are not listed in the standard literature,[51] including those for B, Si, S (for $NTf_2^-$), and $N^-$ (for $NTf_2^-$), we previously reported an arbitrary estimated value for the $NTf_2^-$ volume.[44] Here we report the volumes for $BF_4^-$, $N(SO_2)_2^-$ in $NTf_2^-$, and the TMSiM group of $MTMSiMIm^+$ that are estimated by Bondi's method.[52] The NP group in $MNPIm^+$ is also estimated by Bondi's method to be consistent with the value for the TMSiM group in $MTMSiMIm^+$. We also note that the values used for the van der Waals radii of $B^-$ and $N^-$ are the neutral values.

**3.2. Density Functional Theory of Electronic Structure Calculations.** Figure 2 shows the optimized geometries of $MTMSiMIm^+$ and $MNPIm^+$ with the total electron densities for the isodensity surfaces set at a value of 0.1. As shown in Figure 2, the total electron density distributions of $MTMSiMIm^+$ and $MNPIm^+$ are similar, except for the center atoms of the side groups of the imidazolium cations. The electron density of the Si atom in $MTMSiMIm^+$ is lower than that of the central quaternary C atom of the NP group in $MNPIm^+$. The DFT calculation result shows two major differences between $MTMSiMIm^+$ and $MNPIm^+$. First, the magnitude of atomic charge on the Si atom of $MTMSiMIm^+$ is much larger than that of quaternary C of the NP group in $MNPIm^+$ (+0.772 for $MTMSiMIm^+$ and +0.602 for $MNPIm^+$ from CHelpG calculations). Second, the Si−C bond length for the TMSiM group of $MTMSiMIm^+$ is much longer than that of the C−C for the NP group of $MNPIm^+$: $l$(Si−C) = 1.876 Å and $l$(C−C) = 1.542 Å. The Cartesian coordinates, normal mode vibrational analyses, and CHelpG model atomic charges for the geometry optimized $MTMSiMIm^+$ and $MNPIm^+$ are summarized in the Supporting Information.

**3.3. Optical Kerr Transients and Fourier Transform Spectra.** Figure 3 shows the log−log plots for the Kerr transients for (a) $MTMSiMIm^+/BF_4^-$, (b) $MTMSiMIm^+/NTf_2^-$, (c) $MNPIm^+/BF_4^-$, and (d) $MNPIm^+/NTf_2^-$. For the longest time scale in the observed transients, a triexponential function is used to fit the data in the range of from 3 to 740 ps, although a model function resulting from mode coupling theories can fit nearly as well.[42] Because the longest time constants $\tau_3$ for the $BF_4^-$ IL Kerr transients are about 1 and 4 ns, longer than the experimentally measured time window, it is not possible to unambiguously differentiate between models. The fit curves are also shown in Figure 3. The fit parameters for the triexponential fits are summarized in Table 2. The fast and intermediate

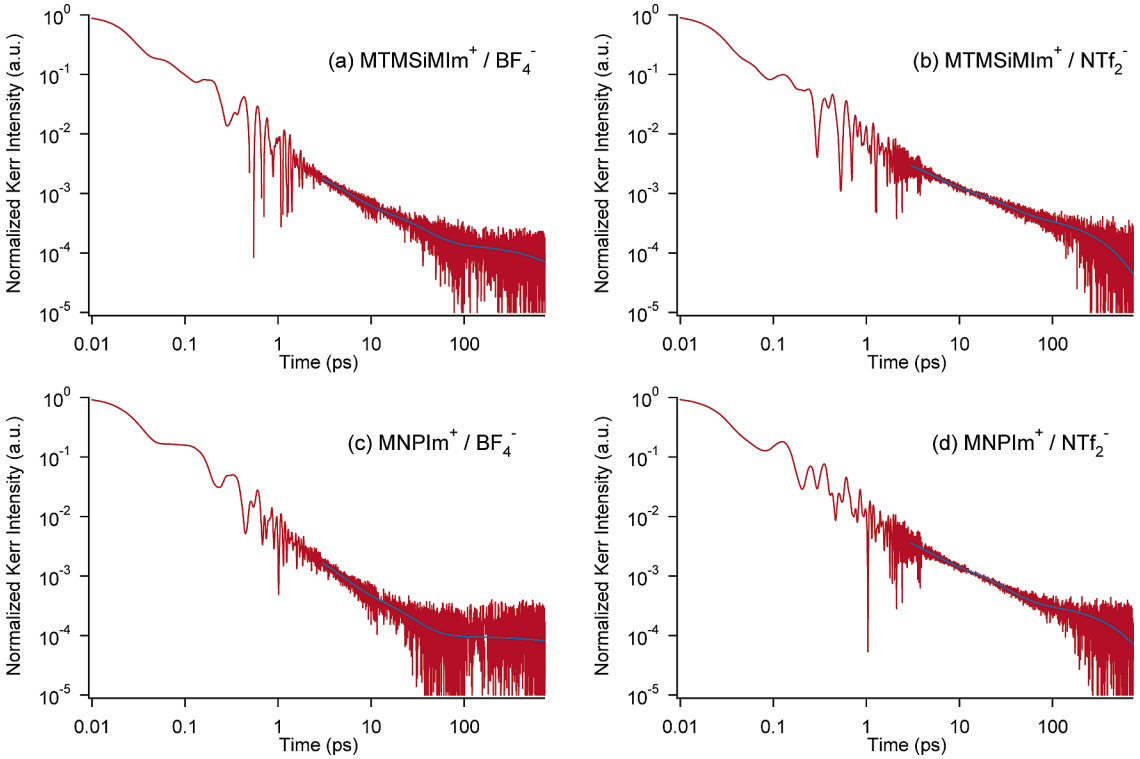


**Figure 3.** Kerr transients of (a) $MTMSiMIm^+/BF_4^-$, (b) $MTMSiMIm^+/NTf_2^-$, (c) $MNPIm^+/BF_4^-$, and (d) $MNPIm^+/NTf_2^-$. Triexponential fit functions are also shown as blue lines.

**TABLE 2: Fit Parameters for Picosecond Kerr Transients of the Room Temperature Ionic Liquids at 296 K**

| liquid | $a_1$[a,b] | $\tau_1$[c] (ps) | $a_2$[a,d] | $\tau_2$[e] (ps) | $a_3$[a,f] | $\tau_3$ (ps) |
|---|---|---|---|---|---|---|
| $MTMSiMIm^+/BF_4^-$ | 0.00339 | 2.56 | 0.00066 | 20.79 | 0.00014 | 1041[g] |
| $MNPIm^+/BF_4^-$ | 0.00406 | 2.17 | 0.00065 | 14.81 | 0.00010 | 4048[g] |
| $MTMSiMIm^+/NTf_2^-$ | 0.00464 | 2.59 | 0.00123 | 18.99 | 0.00045 | 317[h] |
| $MNPIm^+/NTf_2^-$ | 0.00653 | 2.30 | 0.00173 | 17.16 | 0.00037 | 447[h] |

[a] The relative values to the instantaneous electronic response intensity. [b] ±10%. [c] ±10%. [d] ±15%. [e] ±20%. [f] ±30%. [g] ±50%. [h] ±30%.

relaxation time constants, $\tau_1$ and $\tau_2$, do not vary greatly among the four RTILs. On the other hand, the slow relaxation time constant $\tau_3$ is very different for each RTIL.

The shorter time window Kerr transients are analyzed by using the established Fourier transform deconvolution procedures.[28,29] The complete Kerr spectrum is obtained by Fourier transform deconvolution. Subsequently, the Lorentzian components arising from the triexponential relaxation are subtracted to yield a spectrum that emphasizes the femtosecond dynamics. Figure 4 shows the Fourier transform Kerr spectra of (a) $MTMSiMIm^+/BF_4^-$, (b) $MNPIm^+/BF_4^-$, (c) $MTMSiMIm^+/NTf_2^-$, and (d) $MNPIm^+/NTf_2^-$. As shown in Figure 4, the Kerr spectra are well resolved to 700 $cm^{-1}$. Because of the spherical symmetry ($T_d$ point group) for $BF_4^-$, only the two low-frequency depolarized bending modes are observed at 353 and 522 $cm^{-1}$ within the OHD-RIKES spectral window of 0−700 $cm^{-1}$. The two cations and the $NTf_2^-$ anion each contribute to a rich OHD-RIKES spectrum. The intramolecular vibrational mode assignments based on the DFT normal mode calculations and spectra previously reported in the literature[53,54] for $NTf_2^-$ are listed in Table 3. Note that there are several intramolecular normal vibrational modes below 200 $cm^{-1}$ that are superposed atop the intermolecular bands in the 0 to 150 $cm^{-1}$ spectral region.

Figure 5 shows the results from a line shape analysis of the low-frequency Kerr spectra in the frequency range from 0 to 190 $cm^{-1}$ for (a) $MTMSiMIm^+/BF_4^-$, (b) $MTMSiMIm^+/NTf_2^-$, (c) $MNPIm^+/BF_4^-$, and (d) $MNPIm^+/NTf_2^-$. The intermolecular portions of the Kerr spectra are frequently fit to sums of an Ohmic function (eq 5) and two antisymmetrized Gaussian functions, (eq 6) or to related functions.[32,37,40,41,55−65] An additional antisymmetrized Gaussian function, sometimes with one or two additional Lorentzian functions, must be added to fit the specific intramolecular normal modes of the cations and anions. Specifically, the cation modes at 108/97 $cm^{-1}$ for $MTMSiMIm^+$ and at 128/126 $cm^{-1}$ for $MNPIm^+$ are fit to an antisymmetrized Gaussian, while the $NTf_2^-$ torsional mode at 121 $cm^{-1}$ [43,44] and the 180/177 $cm^{-1}$ mode for $MTMSiMIm^+$ are fit to Lorentzians. These complex combinations of line shape functions provided the best fits to the Kerr spectra for the present imidazolium liquids. However, we and others have successfully used sums of Brownian oscillators to fit the intermolecular portions of Kerr spectra for RTILs and other liquids.[38,43,44,65−70] Connecting the intermolecular dynamical spectrum to a predictive theory is still a challenging research problem for much simpler molecular liquids such as benzene,[71] so accurate assignment of the intermolecular modes in complex liquids such as the RTILs discussed here will require comparison with highly accurate molecular dynamics computer simulations. Thus, we recognize that the choice of line shapes is somewhat arbitrary, but proceed with the analysis nonetheless to provide an accurate analytic representation of the experimental data. The broad low-frequency spectra are fit by the sum of an Ohmic function

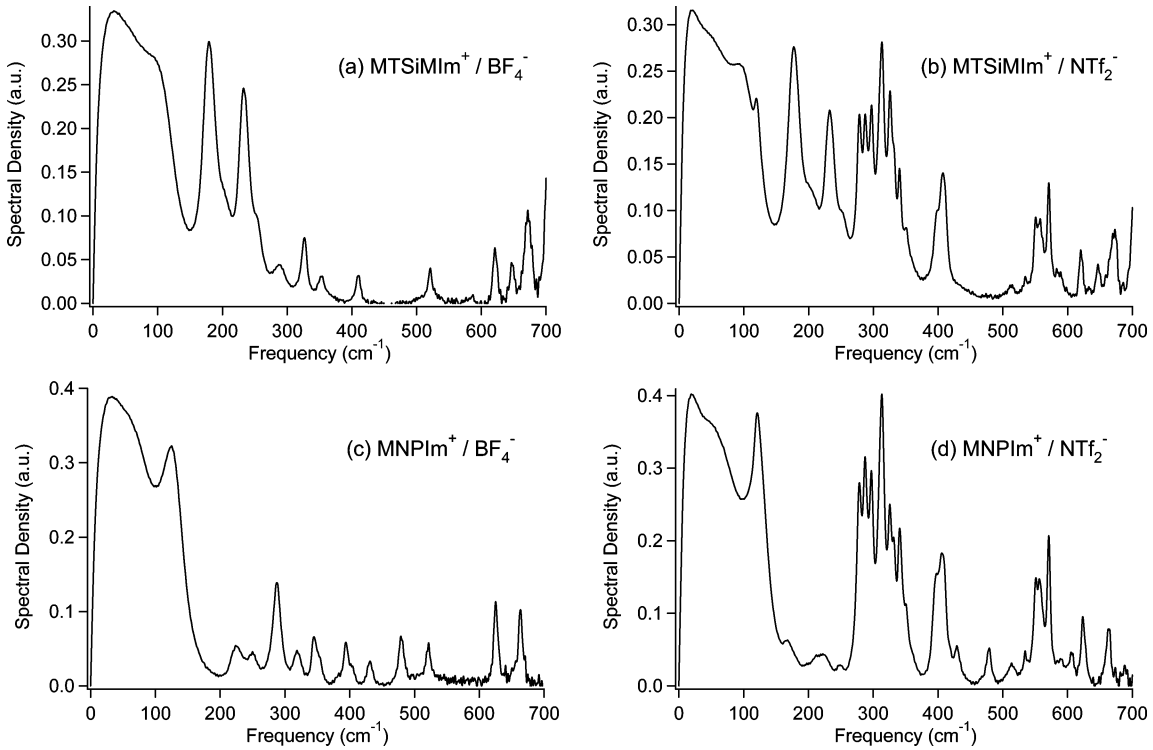


**Figure 4.** Fourier transform Kerr spectra of (a) $MTMSiMIm^+/BF_4^-$, (b) $MTMSiMIm^+/NTf_2^-$, (c) $MNPIm^+/BF_4^-$, and (d) $MNPIm^+/NTf_2^-$.

**TABLE 3: Intramolecular Vibrational Band Frequencies Observed in the Fourier Transform Kerr Spectra of Ionic Liquids**

| $MTMSiMIm^+/BF_4^-$ ($cm^{-1}$) | $MNPIm^+/BF_4^-$ ($cm^{-1}$) | $MTMSiMIm^+/NTf_2^-$ ($cm^{-1}$) | $MNPIm^+/NTf_2^-$ ($cm^{-1}$) | assignment |
|---|---|---|---|---|
| 108 | | 97 | | $MTMSiMIm^+$ |
| | | 121 | 121 | $NTf_2^-$ |
| | 128 | | 126 | $MNPIm^+$ |
| | | | 171 | $NTf_2^-$ |
| 180 | | 177 | | $MTMSiMIm^+$ |
| | 224 | | 218 | $MNPIm^+$ |
| 232 | | 233 | | $MTMSiMIm^+$ |
| | 250 | | 249 | $MNPIm^+$ |
| | | 278 | 279 | $NTf_2^-$ |
| | | 287 | 287 | $NTf_2^-$ |
| | 287 | | | $MNPIm^+$ |
| 288 | | | | $MTMSiMIm^+$ |
| | | 297 | 297 | $NTf_2^-$ |
| | | 313 | 313 | $NTf_2^-$ |
| | 319 | | | $MNPIm^+$ |
| | | 326 | 325 | $NTf_2^-$ |
| 327 | | | | $MTMSiMIm^+$ |
| | | 331 | 331 | $NTf_2^-$ |
| | | 340 | 341 | $NTf_2^-$ |
| | 345 | | | $MNPIm^+$ |
| | | 351 | 350 | $NTf_2^-$ |
| 353 | 354 | | | $BF_4^-$ |
| | 394 | | | $MNPIm^+$ |
| | | 399 | 398 | $NTf_2^-$ |
| | 403 | | | $MNPIm^+$ |
| | | 408 | 406 | $NTf_2^-$ |
| 410 | | | | $MTMSiMIm^+$ |
| | 431 | | 429 | $MNPIm^+$ |
| | 479 | | 479 | $MNPIm^+$ |
| | | 514 | 512 | $NTf_2^-$ |
| 521 | 522 | | | $BF_4^-$ |
| | | 535 | 534 | $NTf_2^-$ |
| | | 551 | 551 | $NTf_2^-$ |
| | | 558 | 556 | $NTf_2^-$ |
| | | 571 | 571 | $NTf_2^-$ |
| 621 | | 620 | | $MTMSiMIm^+$ |
| | 625 | | 624 | $MNPIm^+$ |
| 647 | | 647 | | $MTMSiMIm^+$ |
| | 664 | | 664 | $MNPIm^+$ |
| 672 | | 672 | | $MTMSiMIm^+$ |

(eq 5), two antisymmetrized Gaussian functions (eq 6), and a sum of antisymmetrized Gaussian and Lorentzian functions for several low-frequency intramolecular modes (eq 7):[56−58]

$$I_{\mathrm{Ohmic}}(\omega) = a_{\mathrm{Ohmic}}\omega \exp\left(\frac{-\omega}{\omega_{\mathrm{Ohmic}}}\right) \tag{5}$$

$$I_{\mathrm{G}}(\omega) = \sum_{i=2} a_{\mathrm{G,i}} \exp\left[\frac{-2(\omega - \omega_{\mathrm{G,i}})^2}{(\Delta\omega_{\mathrm{G,i}})^2}\right] - a_{\mathrm{G},i} \exp\left[\frac{-2(\omega + \omega_{\mathrm{G,i}})^2}{(\Delta\omega_{\mathrm{G,i}})^2}\right] \tag{6}$$

$$I_{\mathrm{Intra}}(\omega) = a_{\mathrm{G,Intra}}\left\{\exp\left[\frac{-2(\omega - \omega_{\mathrm{G,Intra}})^2}{(\Delta\omega_{\mathrm{G.Intra}})^2}\right] - \exp\left[\frac{-2(\omega + \omega_{\mathrm{G,Intra}})^2}{(\Delta\omega_{\mathrm{G,Intra}})^2}\right]\right\} + \sum_{i=0,1,2} \frac{a_{\mathrm{L,i}}}{(\omega - \omega_{\mathrm{L,i}})^2 + (\Delta\omega_{\mathrm{L,i}})^2} \tag{7}$$

In eq 5, $a_{\mathrm{Ohmic}}$ and $\omega_{\mathrm{Ohmic}}$ are the amplitude factor and characteristic frequency of an Ohmic line shape. The parameters $a_{\mathrm{G,i}}$, $\omega_{\mathrm{G,i}}$, and $\Delta\omega_{\mathrm{G,i}}$ in eq 6 are the amplitude, peak frequency, and width of an antisymmetrized Gaussian line shape function. The parameters $a_{\mathrm{G,Intra}}$, $\omega_{\mathrm{G,Intra}}$, and $\Delta\omega_{\mathrm{G,Intra}}$ in eq 7 are the amplitude, peak frequency, and width of an antisymmetrized Gaussian line shape function, and the $a_{\mathrm{L,i}}$, $\omega_{\mathrm{L,i}}$, and $\Delta\omega_{\mathrm{L,i}}$ in eq 7 are the Lorentzian amplitudes, center frequencies, and width parameters. The fit parameters are summarized in Table 4. Of course, the other low-frequency *intramolecular* vibrational modes, such as torsional motions, likely are located in this same frequency range. The complete table of intramolecular vibrational normal-mode frequencies from the DFT calculations is provided in the Supporting Information. However, the broad, dominant contributions to the spectrum in this frequency range

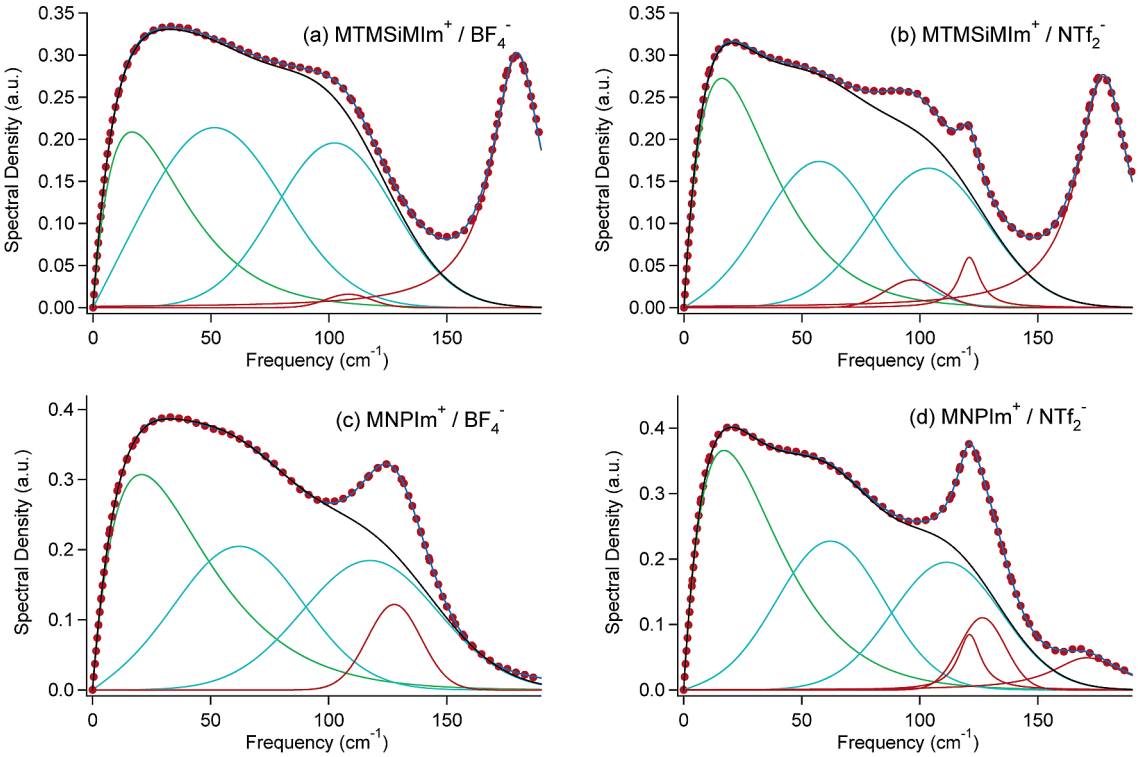


**Figure 5.** Low-frequency broad Kerr spectra and fit functions for (a) $MTMSiMIm^+/BF_4^-$, (b) $MTMSiMIm^+/NTf_2^-$, (c) $MNPIm^+/BF_4^-$, and (d) $MNPIm^+/NTf_2^-$. Red dots denote the data, blue solid lines denote the complete fits, green solid lines denote the Ohmic functions (eq 5), light blue solid lines denote the antisymmetrized Gaussian functions (eq 6), red solid lines denote the antisymmetrized Gaussian or Lorentzian functions for the intramolecular vibrational modes (eq 7), and black solid lines denote the intermolecular contributions (sum of eqs 5 and 6).

**TABLE 4: Fit Parameters for Low-Frequency Kerr Spectra of Each of the Four Room Temperature Ionic Liquids**

(A) Fit Parameters for Intermolecular Spectral Line Shapes

| ionic liquid | $M_1$ ($cm^{-1}$) | $a_{Ohmic}$[a] | $\omega_{Ohmic}$[b] ($cm^{-1}$) | $A_{Ohmic}$ (%) | $a_{G,1}$[c] | $\omega_{G,1}$[d] ($cm^{-1}$) | $\Delta\omega_{G,1}$[e] ($cm^{-1}$) | $A_{G,1}$ (%) | $a_{G,2}$[f] | $\omega_{G,2}$[g] ($cm^{-1}$) | $\Delta\omega_{G,2}$[h] ($cm^{-1}$) | $A_{G,2}$ (%) |
|---|---|---|---|---|---|---|---|---|---|---|---|---|
| $MTMSiMIm^+/BF_4^-$ | 65.8 | 0.034 | 16.5 | 25.9 | 0.214 | 51.3 | 58.3 | 39.9 | 0.196 | 102.4 | 50.3 | 34.1 |
| $MNPIm^+/BF_4^-$ | 71.1 | 0.040 | 20.7 | 39.1 | 0.205 | 62.1 | 54.0 | 30.8 | 0.185 | 117.5 | 57.5 | 30.1 |
| $MTMSiMIm^+/NTf_2^-$ | 63.1 | 0.046 | 16.1 | 36.8 | 0.174 | 57.4 | 47.0 | 31.3 | 0.166 | 103.8 | 49.6 | 31.9 |
| $MNPIm^+/NTf_2^-$ | 64.3 | 0.058 | 17.1 | 41.3 | 0.227 | 62.2 | 45.3 | 31.1 | 0.195 | 111.4 | 46.4 | 27.6 |

(B) Fit Parameters for Intramolecular Spectral Line Shapes.

| ionic liquid | $a_{G,Intra}$ | $\omega_{G,Intra}$ ($cm^{-1}$) | $\Delta\omega_{G,Intra}$ ($cm^{-1}$) | $a_{L,1}$ | $\omega_{L,1}$ ($cm^{-1}$) | $\Delta\omega_{L,1}$ ($cm^{-1}$) | $a_{L,2}$ | $\omega_{L,2}$ ($cm^{-1}$) | $\Delta\omega_{L,2}$ ($cm^{-1}$) |
|---|---|---|---|---|---|---|---|---|---|
| $MTMSiMIm^+/BF_4^-$ | 0.016[i] | 108.4[i] | 19.2[i] | 50.76[i] | 179.9[i] | 13.0[i] | | | |
| $MNPIm^+/BF_4^-$ | 0.129[j] | 127.8[j] | 22.7[j] | | | | | | |
| $MTMSiMIm^+/NTf_2^-$ | 0.033[i] | 97.2[i] | 23.2[i] | 1.68[k] | 120.9[k] | 5.3[k] | 49.45[i] | 177.8[i] | 13.4[i] |
| $MNPIm^+/NTf_2^-$ | 0.110[j] | 126.6[j] | 19.4[j] | 2.87[k] | 121.1[k] | 5.8[k] | 15.46[k] | 170.8[k] | 17.7[k] |

[a] Error is ±15%. [b] Error is ±10%. [c] Error is ±10%. [d] Error is ±5%. [e] Error is ±7%. [f] Error is ±10%. [g] Error is ±5%. [h] Error is ±7%. [i] $MTMSiMIm^+$ intramolecular modes. [j] $MNPIm^+$ intramolecular mode. [k] $NTf_2^-$ intramolecular modes.

arise from *intermolecular* vibrations. The first moments $M_1$ of the broad low-frequency spectra are given by

$$M_1 = \frac{\int_{-\infty}^{+\infty} \omega I(\omega)\, d\omega}{\int_{-\infty}^{+\infty} I(\omega)\, d\omega} \qquad (8)$$

where $I(\omega)$ is the line shape of the intermolecular vibrational spectrum.[72] $M_1$ values are also listed in Table 4.

## 4. Discussion

**4.1. Shear Viscosities.** As shown in Figure 1 and Table 1, the viscosities at room temperature for the $MTMSiMIm^+$ ILs are substantially lower than those for the $MNPIm^+$ ILs: a factor of 1.6 times lower for the $NTf_2^-$ ILs and 7.4 times lower for the $BF_4^-$ ILs. The substantial viscosity reduction resulting from introduction of a TMSiM side group likely arises from several factors. The electrical interactions with neighboring ions will be different for TMSiM vs NP groups, and the volume of the TMSiM side group is larger than that of the NP group. It is likely that the torsional potentials are lower for the TMSiM group than the NP group, which may in turn lead to a greater multiplicity of orientations at a given temperature, further inhibiting ion packing in the liquid. All four of the RTILs reported here show non-Arrhenius viscosity profiles. The viscosity vs temperature graphs can be fit well to the V-T-F model for the liquid shear viscosity.[50] Though apparently excellent fits to the V-T-F model are obtained, with values of $T_0$ ranging from 187 to 202 K, our experimental temperature range from 283 to 363 K is much higher than the strongly

supercooled liquid range, so the $T_0$ values cannot be regarded with a high degree of accuracy.

**4.2. Cation Electronic Structures.** The interaction energies between ions in these RTILs do not appear to be dominated simply by charge−charge interactions. The electrostatics from DFT calculations imply that polarizability effects and substantial effective dipoles (charge arms) will also make substantial contributions to the gas-phase pair interaction energies. Screening effects for the non-uniform fluid, analogous to those giving rise to the Madelung constant in crystal salts, will also complicate accurate calculation of the liquid interaction energies. Nonetheless, it is worth considering the differences in electrostatics for the $MTMSiMIm^+$ and $MNPIm^+$ cations. Unlike the pyrrolidinium RTILs we have recently reported,[44] the imidazolium cation charges are delocalized across the ring system for dialkylimidazoliums such as $MTMSiMIm^+$ and $MNPIm^+$. A carefully selected isodensity plot of the electrostatic potential surface shown in Figure 2 reveals that the positive charge density is highest for the central Si or C atom of the TMSiM and NP side groups.

The atom-centered charges obtained from the CHelpG model for both $MTMSiMIm^+$ and $MNPIm^+$ provided both expected and surprising results. Because of the substantial electronegativity difference between Si and C, we were not surprised to find that the CHelpG charges for the Si atom in $MTMSiMIm^+$ and the central C atom in the NP group of $MNPIm^+$ had values of +0.77 vs +0.60, respectively. What was unexpected was the finding that the sum of the CHelpG charges was nearly identical for the component groups of the two cations: the net charges for the imidazolium rings, and the charges for the TMSiM vs NP groups differed by less than 2% (which we believe is likely to be within the error range for the CHelpG algorithm when used with the default sparse number of data points for the electrostatic potential surface grid).

The DFT calculation results confirm that the Si−C bond lengths on the TMSiM side group are more than 20% longer than the C−C bond lengths of the analogous NP side group (Si−C: 1.876 Å and C−C: 1.542 Å). The larger charge on the TMSiM silicon atom relative to the central NP carbon atom means that the surrounding methyl groups on the TMSiM substituent carry about 50% more electron density than the analogous NP methyl groups: the charge totals for the three methyl groups on the TMSiM group have an average value of −0.15 charge, while the NP methyl groups carry only −0.108 charge. The TMSiM Si−Me bond dipoles are greater than for the case of NP C-Me bonds, and the greater net charges over a larger distance imply a larger polarizability for the TMSiM group relative to the NP group. Thus the principal difference in electronic structure between the $MTMSiMIm^+$ and $MNPIm^+$ cations arises only from differences between the TMSiM and NP functional groups. The TMSiM group is larger, locally more polar, and more polarizable than the NP group in the gas phase, and most of these electronic properties should be observed to be similar in the liquid state of RTILs, though the electronic structure of each ion will be noticeably perturbed by the fields of the surrounding ions. Considering intermolecular interactions with the simplest case of a quasirigid spherical symmetry anion such as $BF_4^-$, one can see that if the gas-phase electronic structure results hold true for the liquid, the cation−anion electrical interactions will be weaker for $MTMSiMIm^+$ than for $MNPIm^+$.

The fact that intermolecular interactions are weaker for $MTMSiMIm^+$ liquids than for $MNPIm^+$ liquids can be understood because the methylimidazolium geometries and net charges are nearly identical for the two cations. While the same effective charge is distributed over the TMSiM and NP side groups, the TMSiM group is larger in volume and is more polarizable than the NP group. Hence the anion−TMSiM interactions should be weaker than the anion−NP interactions and overall the anion−$MTMSiMIm^+$ interactions should be weaker than anion−$MNPIm^+$ interactions. Assuming this simplistic interpretation is correct, the weaker intermolecular interactions suggested from electronic structure results may correlate directly with the reduced frequencies for intermolecular modes observed in the Kerr spectra and the reduced viscosities observed for the $MTMSiMIm^+$ vs the $MNPIm^+$ RTILs (vide infra).

Kobrak and Sandalow illustrated how the "charge-arm" (the distance between the centers of mass and charge, multiplied by the ion charge) can be used for consideration of ionic species in analogy with the way that dipole moments are used to characterize neutral molecules.[73] They speculate that increasing the "charge-arm" of an ion may lead to increased mobility and lower viscosity. Preliminary results indicate that the "charge-arm" for $MTMSiMIm^+$ is about 20% larger than that for $MNPIm^+$.

**4.3. Picosecond Reorientational Kerr Relaxation.** The longest time scale dynamics observed in the fs-OHD-RIKES experiment are relaxation processes occurring on time scales of picoseconds to nanoseconds. Triexponential models fit marginally better than mode-coupling theory equations, which are shown to work well for the 1-ethyl-3-methylimidazolium nitrate RTIL by Fayer and co-workers.[42] For each of the four imidazolium cation ILs considered here, the fastest and intermediate relaxation time constants $\tau_1$ and $\tau_2$ are invariant to within the uncertainties of the fitting procedure at 296 K. Interestingly, similar time scale relaxation processes have also been observed in the other RTILs having different pairs of cations and anions.[43,44]

The slowest relaxation time constant $\tau_3$ shows dramatic variations among the time constants for these four RTILs. Interestingly, similar time scale relaxation processes have also been observed in the other RTILs having different pairs of cations and anions.[43,44] It is possible that these relaxations result from the reorientations of the individual cation and anion constituents. It is important to point out that reorientation of an individual $BF_4^-$ anion will not contribute to the Kerr signal because of the spherical $T_d$ symmetry of this anion. However, clusters containing the $BF_4^-$ anion will not have this spherical symmetry, so they can contribute to reorientation signals if the cluster lifetime exceeds the jump diffusion time scale.

Figure 6 plots the longest Kerr relaxation time constant $\tau_3$ versus the product of the shear viscosity times the volume for each of the RTILs, except for $MNPIm^+/BF_4^-$. The reason for rejecting the $MNPIm^+/BF_4^-$ $\tau_3$ data point is that the time constant obtained from the triexponential nonlinear least-squares fit is much larger than the measurement time window of 740 ps. The graph abscissa is the measured shear viscosity multiplied by the van der Waals volume of one element from the set of anion, cation, cation:anion pair, 2-cation:anion cluster, and cation:2-anion cluster. It is apparent on inspection of the graph that there is no correlation between $\tau_3$ and viscosity−$V$(anion). Of course, one could expect that the comparison between the two $NTf_2^-$ RTILs and the $MTMSiMIm^+/BF_4^-$ liquid might not be appropriate. However, the correlations between the cation and cluster data suggest that this comparison may in fact be worthwhile. Reasonable correlations are seen for the graphs of $\tau_3$ vs the viscosity−volume product for each of the other

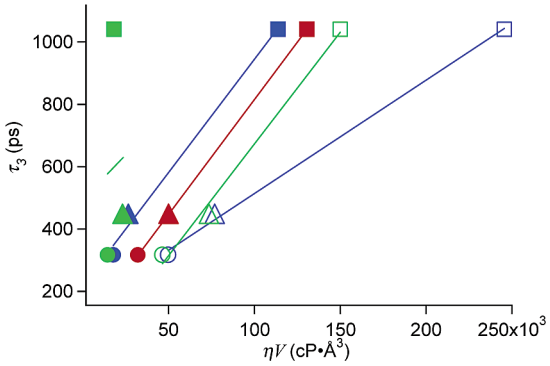


**Figure 6.** Plots of $\tau_3$ vs $\eta V$ for MTMSiMIm$^+$/NTf$_2^-$, MNPIm$^+$/NTf$_2^-$, and MTMSiMIm$^+$/BF$_4^-$. Green, blue, and red filled symbols represent points calculated with use of the molecular volumes of the anion, cation, and the sum of cation and anion, respectively. The plots shown with open green and blue symbols result from using the molecular volumes of the cation:2-anion and 2-cation:anion clusters, respectively. Circles, triangles, and squares are MTMSiMIm$^+$/NTf$_2^-$, MNPIm$^+$/NTf$_2^-$, and MTMSiMIm$^+$/BF$_4^-$, respectively. The solid lines are least-squares fits to the data.

elements of the above set, with a remarkably strong correlation observed for the cation:anion pair. While it is not reasonable to draw strong conclusions from a set of three reorientation time constants, we believe that the data shown in Figure 6 show that it is likely that the orientational relaxation observed in the Kerr data does provide evidence for reorientation of clusters that persist for longer than the orientational jump diffusion time constant.

Several molecular dynamics simulation studies of the RTIL dynamics have shown that the anion and cation motions are strongly coupled.[74,75] An NMR study of the ion diffusions of *N*-butylpyridinium and 1-ethyl-3-methylimidazolium cation ILs with NTf$_2^-$ and BF$_4^-$ anion showed that the sum of the diffusion coefficients of anion and cation is well correlated with the inverse of the viscosity.[76] Clear experimental evidence for RTIL ion clustering in the gas phase results from ESI-MS studies, for which positively charged (cation)$_{n+1}$:(anion)$_n$ clusters were detected for $n = 2-5$.[77] This implies that these cluster species must be stable for at least the microsecond duration of the MS experiment, if not for much longer time scales. Our ESI-MS results also confirm the presence of 2:1 positive and negative ion clusters. Dielectric relaxation experiments show broad distributions of relaxation phenomena in the ethylammonium nitrate IL that have been attributed to an 8% contribution from contact ion pair reorientation.[78] Therefore, it is plausible that diffusive relaxation signals from optical Kerr experiments may be comprised of a sum of individual cation and anion reorientations, as well as cation−anion pairs and higher order charged and neutral ion clusters.

On the other hand, the solvent reorganization process in RTILs measured with fluorescence probes (solvation dynamics via the time-dependent fluorescence Stokes shift) shows a substantial amplitude of the slow component on the nanosecond time scale.[79−85] Because of the differences in length and time scales that are probed, and the likelihood for specific solvation effects,[74,86] we do not expect to find simple correlations between the solvation dynamics measured by time-resolved fluorescence Stokes shifts and Kerr polarizability anisotropy dynamics. For example, fluorescence probing could be sensitive to longer time scale translational diffusion processes that effect ion exchanges because the fluorescence probe solvatochromism provides an effective step-function change in the electrical environment of the RTIL being probed. In contrast, OHD-RIKES transients measure the bath fluctuations on the fastest time scales to a femtosecond duration impulse response. Simply put, the complex structural and dynamical features observed in RTILs require that we check whether the linear response approximation is valid.

The polarizability anisotropy relaxation of *N*-ethoxyethyl-*N*-methylpyrrolidinium bromide has also shown similar time scale relaxations for $\tau_1$ and $\tau_2$ (1.89 and 21.2 ps).[44] Therefore, these relaxation processes are unlikely due to the reorientations of each constituent of the RTIL. Possible origins for the relaxation could be the power-law processes invoked in mode-coupling theory,[42] intermolecular vibrational relaxation,[87−90] and non-Markovian relaxation processes.[91] Temperature-dependent experiments may provide insight into the origin of these fast and intermediate relaxation processes.

**4.4. Intermolecular Vibrational Dynamics.** The low-frequency spectral region from 0 to 200 cm$^{-1}$ usually is dominated by the intermolecular vibrational dynamics for most neutral organic liquids. The same is true for RTILs, but the spectra are often shifted to somewhat higher frequencies. The substantial flexibility of the RTIL cations and anions often leads to low-frequency modes that also are found in the same low-frequency region of the spectrum. Figure 5 shows how sharper Lorentzian features arising from the cation and anion intramolecular normal modes are superposed with the broad "blob" spectra in the 0 to 150 cm$^{-1}$ spectral range. For strongly dipolar liquids such as acetonitrile, the dominant contributions to the intermolecular vibrational dynamics result primarily from librational and density fluctuation dynamics, with the former dominating the spectral density.[71,92−95] Because these motions have strong overlap in time scales, and are in fact likely coupled for such flexible, strongly interacting ions as those in the RTILs reported here, it is difficult to distinguish between them. It is quite likely that the features fit to eqs 5 and 6 cannot be correlated directly with any simple decomposition of the line shape into orientational and translational dynamics.

From the intermolecular line shape features shown in Figure 5 and corresponding fit parameters listed in Table 4, we find two interesting points. (1) The peak frequencies of all the modes for MTMSiMIm$^+$ ILs are lower than those for MNPIm$^+$ ILs. The $M_1$ frequencies are also lower for the silicon-substituted imidazolium cation RTILs than for the alkyl-substituted ones. (2) The magnitude of the differences for the intermolecular frequencies and the spectral first moments $M_1$ that are parametrized in Table 4 is larger for the BF$_4^-$ ILs than for the NTf$_2^-$ ILs. Considering both the peak frequencies for the intermolecular line shapes and the $M_1$ values for each of the four RTILs, we find that the MTMSiMIm$^+$ frequencies are uniformly lower than those for MNPIm$^+$, both for the BF$_4^-$ and the NTf$_2^-$ cases. We recall that the room temperature viscosity ratios $\eta$(MNPIm$^+$)/$\eta$(MTMSiMIm$^+$) are 7.4:1 for ILs with the BF$_4^-$ anion, and 1.6:1 for the ILs with the NTf$_2^-$ anion. The magnitude of the frequency differences seems to correlate with viscosity, because the value of the $M_1$(MNPIm$^+$) is 8% higher than $M_1$(MTMSiMIm$^+$) for the BF$_4^-$ anion ILs, but only 2% higher for NTf$_2^-$ anion ILs.

The silicon-substituted MTMSiMIm$^+$ cation has a larger molecular volume by 13.4 Å$^3$ than the corresponding MNPIm$^+$ cation because the Si−C bond lengths are substantially longer than the C−C bonds. Thus, on average, one would expect that the intermolecular interactions between a given anion and MTMSiMIm$^+$ might be weaker than those for MNPIm$^+$. Furthermore, the larger atom-centered charge for the Si atom

of +0.77, vs +0.60 for the corresponding central NP carbon atom, is isolated by the longer bond of Si−C relative to the C−C bond length of the NP group.

Considering a generic vibrational oscillator coordinate, $\omega = (k/\mu)^{1/2}$ where $k$ is the force constant and $\mu$ is the effective mass, we might expect that the frequencies for such an intermolecular mode would be reduced for the $MTMSiMIm^+$ cation relative to the $MNPIm^+$ cation for at least two reasons: (i) The effective mass for the $MTMSiMIm^+$ cation is larger than that for the $MNPIm^+$ cation and (ii) the intermolecular interactions for $MTMSiMIm^+$ ILs are weaker than those for the $MNPIm^+$ ILs. The intermolecular spectrum can be seen to be lower in frequency for the $MTMSiMIm^+$ RTILs than for the analogous $MNPIm^+$ RTILs by both the crude characterization of the low-frequency spectrum by the first spectral moment $M_1$ and by the peak frequencies for each of the Ohmic and two Gaussian intermolecular line shapes fit to the intermolecular spectrum, all listed in Table 4. The magnitude of the difference in frequencies resulting from silicon substitution on the cation does not correlate with the difference in effective masses for either the $NTf_2^-$ or the $BF_4^-$ ILs. Therefore, the difference in effective masses between silicon-substituted and normal IL cations is not the dominant factor in determining intermolecular frequencies in these four RTILs. We expect that liquids with higher viscosities should have stronger intermolecular interactions and thus overall higher frequency intermolecular modes relative to lower viscosity liquids.

## 5. Conclusions

In this study, we report the synthesis and properties of the first of a new class of silicon-substituted imidazolium cation room temperature ionic liquids. The viscosities of the imidazolium RTILs are substantially reduced by replacing a neopentyl group with the analogous trimethylsilylmethyl group. To understand the silicon substitution effect on the viscosity of RTILs, we have performed DFT electronic structure calculations on $MTMSiMIm^+$ and $MNPIm^+$ at the B3LYP/6-311+G(d,p) level of theory and computed the normal vibrational modes and atom-centered charges. Ultrafast dynamics of the RTILs measured by femtosecond OHD-RIKES provide insight into both the diffusive orientational relaxation and the inter- and intramolecular vibrational dynamics. The viscosity data, results from DFT calculations, and characteristic frequencies of the intermolecular vibrational spectra are well correlated. Apparently the interactions between the ions for the $MTMSiMIm^+$ RTILs are weaker than those for the analogous $MNPIm^+$ RTILs.

**Acknowledgment.** We gratefully acknowledge the National Science Foundation for support of this work (CHE-0239390). We thank Dr. James F. Wishart, Dr. Alison M. Funston (Brookhaven National Laboratory), and Prof. Mark N. Kobrak (Brooklyn College) for many stimulating discussions. We thank Dr. Patrick O'Connor and Dr. Alexei Ermakov (Rutgers) for their kind help with NMR and ESI-MS measurements, respectively. We also thank Prof. David S. Talaga (Rutgers) for use of a vacuum oven.

**Supporting Information Available:** Details of the RTIL synthesis procedures along with atomic coordinates, atom-centered charges, and vibrational frequencies at the B3LYP/6-311+G(d,p) level of theory. This material is available free of charge via the Internet at http://pubs.acs.org.

**Note Added in Proof.** Water content in the Kerr samples was minimized by the vacuum oven drying procedure described above, but was not measured at the time of the experiment. Later measurements using Karl Fischer coulometric titration on $MTMSiMIm^+/BF_4^-$ provided a value of 800 ppm, measured after the samples had been exposed to ambient atmosphere, and had thus likely absorbed water. Because the $NTf_2^-$ RTILs are more hydrophobic, we predict that the water content is lower than for $BF_4^-$ ionic liquids.

## References and Notes

(1) Welton, T. *Chem. Rev.* **1999**, *99*, 2071.
(2) Earle, M. J.; Seddon, K. R. *Pure Appl. Chem.* **2000**, *72*, 1398.
(3) Wasserscheid, P.; Keim, W. *Angew. Chem., Int. Ed.* **2000**, *39*, 3772.
(4) Kitazume, T. *J. Fluorine Chem.* **2000**, *105*, 265.
(5) Zhao, H.; V., M. S. *Aldrichim. Acta* **2002**, *35*, 75.
(6) Wilkes, J. S. *Green Chem.* **2002**, *4*, 73.
(7) Dupont, J.; de Souza, R. F.; Suarez, P. A. Z. *Chem. Rev.* **2002**, *102*, 3667.
(8) Forsyth, S. A.; Pringle, J. M.; MacFarlane, D. R. *Aust. J. Chem.* **2004**, *57*, 113.
(9) Davis, J. H., Jr. *Chem. Lett.* **2004**, *33*, 1072.
(10) Riddick, J. A.; Bunger, W. B.; Sakano, T. K. *Organic Solvents, Physical Properties and Method of Purification*, 4th ed.; John Wiley & Sons: New York, 1986.
(11) Bonhote, P.; Sias, A.-P.; Papageorgiou, N.; Kalyanasundaram, K.; Gratzel, M. *Inorg. Chem.* **1996**, *35*, 1168.
(12) MacFarlane, D. R.; Forsyth, S. A.; Golding, J.; Deacon, G. B. *Green Chem.* **2002**, *4*, 444.
(13) Cooper, E. I.; Angell, C. A. *Solid State Ionics* **1983**, *9&10*, 617.
(14) Matsumoto, H.; Yanagida, M.; Tanimoto, K.; Nomura, N.; Kitagawa, Y.; Miyazaki, Y. *Chem. Lett.* **2000**, *922*.
(15) Funston, A. M.; Wishart, J. F. *ACS Symp. Ser.* **2005**, *901*, 102.
(16) Zhao, D.; Fei, Z.; Scopelliti, R.; Dyson, P. J. *Inorg. Chem.* **2004**, *43*, 2197.
(17) Brook, M. A. *Silicon in Organic, Organomethalic, and Polymer Chemistry*; John Wiley & Sons: New York, 2000.
(18) Liebau, F. *Structural Chemistry of Silicates*; Springer-Verlag: Berlin, Germany, 1985.
(19) *Polymer Handbook*, 4th ed.; Brandrup, J., Immergut, E. H., Grulke, E. A., Eds.; John Wiley & Sons: New York, 1999.
(20) Baney, R. H.; Itoh, M.; Sakakibara, A.; Suzuki, T. *Chem. Rev.* **1995**, *95*, 1409.
(21) *Silicon in Polymer Synthesis*; Kricheldorf, H. R., Ed.; Springer: Berlin, Germany, 1996.
(22) Huddleston, J. G.; Wilauer, H. D.; Swatloski, R. P.; Visser, R. D.; Rogers, R. D. *Chem. Commun.* **1998**, 1765.
(23) Holbrey, J. D.; Seddon, K. R. *J. Chem. Soc., Dalton Trans.* **1999**, 2133.
(24) Dzyuba, S. V.; Bartsch, R. A. *J. Heterocycl. Chem.* **2001**, *38*, 265.
(25) Dzyuba, S. V.; Bartsch, R. A. *ChemPhysChem* **2002**, *3*, 161.
(26) McMorrow, D.; Lotshaw, W. T.; Kenney-Wallace, G. A. *IEEE J. Quantum Electron.* **1988**, *24*, 443.
(27) Lotshaw, W. T.; McMorrow, D.; Thantu, N.; Melinger, J. S.; Kitchenham, R. *J. Raman Spectrosc.* **1995**, *26*, 571.
(28) McMorrow, D.; Lotshaw, W. T. *Chem. Phys. Lett.* **1990**, *174*, 85.
(29) McMorrow, D.; Lotshaw, W. T. *J. Phys. Chem.* **1991**, *95*, 10395.
(30) Kinoshita, S.; Kai, Y.; Ariyoshi, T.; Shimada, Y. *Int. J. Mod. Phys. B* **1996**, *10*, 1229.
(31) Castner, E. W., Jr.; Maroncelli, M. *J. Mol. Liq.* **1998**, *77*, 1.
(32) Smith, N. A.; Meech, S. R. *Int. Rev. Phys. Chem.* **2002**, *21*, 75.
(33) Loughnane, B. J.; Farrer, R. A.; Scodinu, A.; Reilly, T.; Fourkas, J. T. *J. Phys. Chem. B* **2000**, *104*, 5421.
(34) Farrer, R. A.; Fourkas, J. T. *Acc. Chem. Res.* **2003**, *36*, 605.
(35) Hunt, N. T.; Jaye, A. A.; Meech, S. R. *J. Phys. Chem. B* **2003**, *107*, 3405.
(36) Hunt, N. T.; Jaye, A. A.; Hellman, A.; Meech, S. R. *J. Phys. Chem. B* **2004**, *108*, 100.
(37) Jaye, A. A.; Hunt, N. T.; Meech, S. R. *Langmuir* **2005**, *21*, 1238.
(38) Shirota, H. *J. Phys. Chem. B* **2005**, *109*, 7053.
(39) Shirota, H.; Castner, E. W., Jr. *J. Am. Chem. Soc.* **2001**, *123*, 12877.
(40) Hyun, B. R.; Dzyuba, S. V.; Bartsch, R. A.; Quitevis, E. L. *J. Phys. Chem. A* **2002**, *106*, 7579.
(41) Rajian, J. R.; Li, S.; Bartsch, R. A.; Quitevis, E. L. *Chem. Phys. Lett.* **2004**, *393*, 372.
(42) Cang, H.; Li, J.; Fayer, M. D. *J. Chem. Phys.* **2003**, *119*, 13017.
(43) Giraud, G.; Gordon, C. M.; Dunkin, I. R.; Wynne, K. *J. Chem. Phys.* **2003**, *119*, 464.
(44) Shirota, H.; Funston, A. M.; Wishart, J. F.; Castner, E. W., Jr. *J. Chem. Phys.* **2005**, *122*, 184512.
(45) Wiewior, P. P.; Shirota, H.; Castner, E. W., Jr. *J. Chem. Phys.* **2002**, *116*, 4643.

(46) Frisch, M. J.; Trucks, G. W.; Schlegel, H. B.; Scuseria, G. E.; Robb, M. A.; Cheeseman, J. R.; Montgomery, J. A., Jr.; Vreven, T.; Kudin, K. N.; Burant, J. C.; Millam, J. M.; Iyengar, S. S.; Tomasi, J.; Barone, V.; Mennucci, B.; Cossi, M.; Scalmani, G.; Rega, N.; Petersson, G. A.; Nakatsuji, H.; Hada, M.; Ehara, M.; Toyota, K.; Fukuda, R.; Hasegawa, J.; Ishida, M.; Nakajima, T.; Honda, Y.; Kitao, O.; Nakai, H.; Klene, M.; Li, X.; Knox, J. E.; Hratchian, H. P.; Cross, J. B.; Adamo, C.; Jaramillo, J.; Gomperts, R.; Stratmann, R. E.; Yazyev, O.; Austin, A. J.; Cammi, R.; Pomelli, C.; Ochterski, J. W.; Ayala, P. Y.; Morokuma, K.; Voth, G. A.; Salvador, P.; Dannenberg, J. J.; Zakrzewski, V. G.; Dapprich, S.; Daniels, A. D.; Strain, M. C.; Farkas, O.; Malick, D. K.; Rabuck, A. D.; Raghavachari, K.; Foresman, J. B.; Ortiz, J. V.; Cui, Q.; Baboul, A. G.; Clifford, S.; Cioslowski, J.; Stefanov, B. B.; Liu, G.; Liashenko, A.; Piskorz, P.; Komaromi, I.; Martin, R. L.; Fox, D. J.; Keith, T.; Al-Laham, M. A.; Peng, C. Y.; Nanayakkara, A.; Challacombe, M.; Gill, P. M. W.; Johnson, B.; Chen, W.; Wong, M. W.; Gonzalez, C.; Pople, J. A. *GAUSSIAN 03*; Gaussian, Inc.: Pittsburgh, PA, 2003.

(47) Becke, A. D. *J. Chem. Phys.* **1993**, *98*, 5648.

(48) Lee, C.; Yang, W.; Parr, R. G. *Phys. Rev. B* **1988**, *37*, 785.

(49) Breneman, C. M.; Wiberg, K. B. *J. Comput. Chem.* **1990**, *11*, 361.

(50) Angell, C. A. *Chem. Rev.* **2002**, *102*, 2627.

(51) Edwards, J. T. *J. Chem. Educ.* **1970**, *47*, 261.

(52) Bondi, A. *J. Phys. Chem.* **1964**, *68*, 441.

(53) Rey, I.; Johansson, P.; Lindgren, J.; Lassegues, L. C.; Grondin, J.; Sevant, L. *J. Phys. Chem. A* **1998**, *102*, 3249.

(54) Castriota, M.; Caruso, T.; Agostino, R. G.; Caszzanelli, E.; Henderson, W. A.; Passeini, S. *J. Phys. Chem. A* **2005**, *109*, 92.

(55) Cho, M.; Du, M.; Scherer, N. F.; Fleming, G. R.; Mukamel, S. *J. Chem. Phys.* **1993**, *99*, 2410.

(56) Chang, Y. J.; Castner, E. W., Jr. *J. Chem. Phys.* **1993**, *99*, 7289.

(57) Chang, Y. J.; Castner, E. W., Jr. *J. Phys. Chem.* **1994**, *98*, 9712.

(58) Chang, Y. J.; Castner, E. W., Jr. *J. Phys. Chem.* **1996**, *100*, 3330.

(59) Smith, N. A.; Lin, S.; Meech, S. R.; Shirota, H.; Yoshihara, K. *J. Phys. Chem. A* **1997**, *101*, 9578.

(60) Smith, N. A.; Lin, S.; Meech, S. R.; Yoshihara, K. *J. Phys. Chem. A* **1997**, *101*, 3641.

(61) Shirota, H.; Yoshihara, K.; Smith, N. A.; Lin, S.; Meech, S. R. *Chem. Phys. Lett.* **1997**, *281*, 27.

(62) Smith, N. A.; Meech, S. R. *J. Phys. Chem. A* **2000**, *104*, 4223.

(63) Shirota, H. *J. Chem. Phys.* **2005**, *122*, 044514.

(64) Ricci, M.; Bartolini, P.; Chelli, R.; Cardini, G.; Califano, S.; Righini, R. *Phys. Chem. Chem. Phys.* **2001**, *3*, 2795.

(65) Beard, M. C.; Lotshaw, W. T.; Korter, T. M.; Heilweil, E. J.; McMorrow, D. *J. Phys. Chem. A* **2004**, *108*, 9348.

(66) Tanimura, Y.; Mukamel, S. *J. Chem. Phys.* **1993**, *99*, 9496.

(67) Palese, S.; Buontempo, J. T.; Schlling, L.; Lotshaw, W. T.; Tamimura, Y.; Mukamel, S.; Miller, R. J. D. *J. Phys. Chem.* **1994**, *98*, 12466.

(68) Palese, S.; Mukamel, S.; Miller, R. J. D.; Lotshaw, W. T. *J. Phys. Chem.* **1996**, *100*, 10380.

(69) Mukamel, S. *Principles of Nonlinear Optical Spectroscopy*; Oxford University Press: New York, 1995.

(70) Giraud, G.; Karolin, J.; Wynne, K. *Biophys. J.* **2003**, *85*, 1903.

(71) Ryu, S.; Stratt, R. M. *J. Phys. Chem. B* **2004**, *108*, 6782.

(72) McHale, J. L. *Molecular Spectroscopy*; Prentice-Hall: Upper Saddle River, NJ, 1999.

(73) Kobrak, M. N.; Sandalow, N. An Electrostatic Interpretation of Structure−Property Relationships in Ionic Liquids. In *Molten Salts XIV*; Mantz, R. A., Ed.; The Electrochemical Society: Pennington, NJ, in press.

(74) Kobrak, M. N.; Znamenskiy, V. *Chem. Phys. Lett.* **2004**, *395*, 127.

(75) Margulis, C. J. *Mol. Phys.* **2004**, *102*, 829.

(76) Noda, A.; Hayamizu, K.; Watanabe, M. *J. Phys. Chem. B* **2001**, *105*, 4603.

(77) Zhao, D. *Aust. J. Chem.* **2004**, *57*, 509.

(78) Weingartner, H.; Knocks, A.; Schrader, W.; Kaatze, U. *J. Phys. Chem. A* **2001**, *105*, 8646.

(79) Karmakar, R.; Samanta, A. *J. Phys. Chem. A* **2002**, *106*, 4447.

(80) Karmakar, R.; Samanta, A. *J. Phys. Chem. A* **2003**, *107*, 7340.

(81) Chakravarty, D.; Harza, P.; Chakravarty, A.; Seth, D.; Sarkar, N. *Chem. Phys. Lett.* **2003**, *381*, 697.

(82) Ingram, J. A.; Moog, R. S.; Ito, N.; Biswas, R.; Maroncelli, M. *J. Phys. Chem. B* **2003**, *107*, 5926.

(83) Ito, N.; Arzhantsev, M.; Heinz, M.; Maroncelli, M. *J. Phys. Chem. B* **2004**, *108*, 5771.

(84) Ito, N.; Arzhantsev, M.; Maroncelli, M. *Chem. Phys. Lett.* **2004**, *396*, 83.

(85) Chowdhury, P. K.; Halder, M.; Sanders, L.; Calhoun, T.; Anderson, J. L.; Armstrong, D. W.; Song, X.; Petrich, J. W. *J. Phys. Chem. B* **2004**, *108*, 10245.

(86) Harper, J. B.; Lynden-Bell, R. M. *Mol. Phys.* **2004**, *102*, 85.

(87) Loughnane, B. J.; Scodinu, A.; Farrer, R. A.; Fourkas, J. T.; Mohanty, U. *J. Chem. Phys.* **1999**, *111*, 2686.

(88) McMorrow, D.; Thantu, N.; Kleiman, V.; Melinger, J. S.; Lotshaw, W. T. *J. Phys. Chem. A* **2001**, *105*, 7960.

(89) McMorrow, D.; Lotshaw, W. T.; Melinger, J. S.; Kleiman, V. *ACS Symp. Ser.* **2002**, *820*, 14.

(90) Scodinu, A.; Fourkas, J. T. *J. Phys. Chem. B* **2003**, *107*, 44.

(91) Fainberg, B. D.; Huppert, D. *J. Mol. Liq.* **1996**, *68*, 281.

(92) Madden, P. A.; Cox, T. I. *Mol. Phys.* **1981**, *43*, 287.

(93) Madden, P. A. In *Molecular Liquids—Dynamics and Interactions*; Barnes, A. J., Orville-Thomas, W. J., Eds.; D. Reidel Publishing Company: Dordrecht, The Netherlands, 1983; p 431.

(94) Geiger, L. C.; Ladanyi, B. M. *J. Chem. Phys.* **1988**, *89*, 6588.

(95) Geiger, L. C.; Ladanyi, B. M. *Chem. Phys. Lett.* **1989**, *159*, 413.

(96) Baker, S. N.; Baker, G. A.; Munson, C. A.; Chen, F.; Bukowski, E. J.; Cartwright, A. N.; Bright, F. V. *Ind. Eng. Chem. Res.* **2003**, *42*, 6457.